

Acid-functionalized UiO-66(Zr) MOFs and their evolution after intra-framework cross-linking: structural features and sorption properties.

Florence Ragon^a, Betiana Campo^b, Qingyuan Yang^{c,d}, Charlotte Martineau^a, Andrew D. Wiersum^e, Ana Lago^a, Vincent Guillerma^a, Callum Hemsley^a, Jarrod F. Eubank^a, Muthusamy Vishnuvarthan^b, Francis Taulelle^a, Patricia Horcajada^a, Alexandre Vimont^b, Philip L. Llewellyn^e, Marco Daturi^b, Sabine Devautour-Vinot^c, Guillaume Maurin^c, Christian Serre^a, Thomas Dovic,^{a,*} Guillaume Clet^{b,*}

(a) Institut Lavoisier, UMR CNRS 8180, Université de Versailles Saint-Quentin-en-Yvelines, 45 avenue des Etats-Unis, 78035 Versailles cedex, France

(b) Laboratoire Catalyse et Spectrochimie, ENSICAEN, Université de Caen Basse-Normandie, CNRS, 6 Bd. du Maréchal Juin, 14050 Caen, France.

(c) Institut Charles Gerhardt Montpellier, UMR CNRS 5253, UM2, ENSCM, Place E. Bataillon, 34095 Montpellier cedex 05, France.

(d) State Key Laboratory of Organic-Inorganic Composites, Beijing University of Chemical Technology, P.O. Box 100 Beijing 100029, China.

(e) Aix-Marseille Univ. - CNRS, Laboratoire MADIREL, UMR 7246, Centre de Saint Jérôme, 13397 Marseille 20, France.

Supplementary Information

1. Synthesis conditions.....	S2
2. Materials characterisations.....	S3
3. Kinetic data.....	S5
4. Modelling.....	S10
5. Gas adsorption.....	S13
References.....	S15

1. Synthesis conditions

Table S1. Synthesis conditions of the HT screening in the system $\text{ZrCl}_4/1,2,4\text{-BTC}$ or $\text{BTeC}/\text{H}_2\text{O}/\text{HCl}(37\%)$ at $100\text{ }^\circ\text{C}$ in 72 h.

1,2,4-BTC BTeC		ZrCl_4		L : M	H_2O V (mL)	HCl (37%) V (mL)	[HCl] M
n (mmol)	m (mg)	n (mmol)	m (mg)				
0.1	21 25	0.3	70	0.3 : 1	1	0	0
					0.5	0.5	6
					0	1	12
0.3	63 76			1 : 1	1	0	0
					0.5	0.5	6
					0	1	12
0.6	126 153			2 : 1	1	0	0
					0.5	0.5	6
					0	1	12
0.9	189 229	3 : 1	0.5	0	0		
			0.5	0.5	6		
			0	1	12		

Table S2. Synthesis conditions to form $\text{UiO-66}(\text{Zr})\text{-(COOH)}$ and $\text{UiO-66}(\text{Zr})\text{-(COOH)}_2$ via the round bottom flask route at $100\text{ }^\circ\text{C}$ in 24 h.

	Ligand	Metallic precursor	H_2O	HCl (37%)
$\text{UiO-66}(\text{Zr})\text{-(COOH)}$	1,2,4-BTC 5 mmol 1.1 g	ZrCl_4 5 mmol 1.2 g	25 mL	0 mL
$\text{UiO-66}(\text{Zr})\text{-(COOH)}_2$	BTeC 5 mmol 1.3 g			

Table S3. Synthesis conditions of the solvothermal reactions to form $\text{UiO-66}(\text{Zr})\text{-(COOH)}$ and $\text{UiO-66}(\text{Zr})\text{-(COOH)}_2$ in pure water or in presence of 7.5 equivalents of HCl (37 %) per Zr .

	1,2,4- BTC	BTeC	ZrCl_4	H_2O	HCl (37 %)
7.5 HCl/Zr	0.4 mmol 85 mg	0.4 mmol 108 mg	0.4 mmol 93 mg	1.75 mL	0.25 mL (1.5 M)

2. Materials characterisations

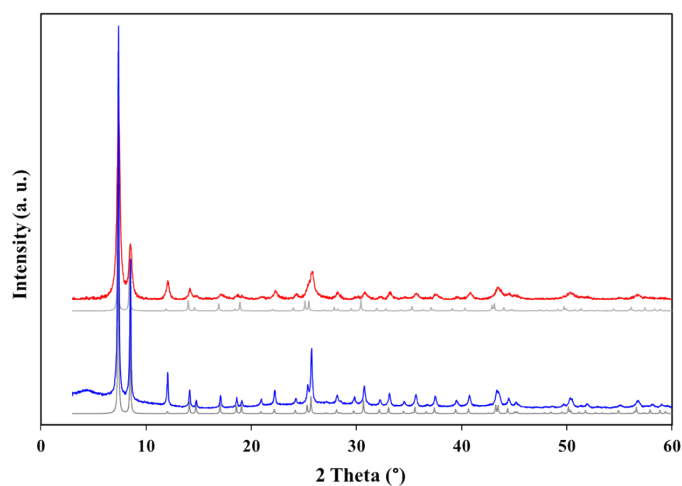


Figure S1. Experimental X-ray powder diffraction patterns of UiO-66(Zr)-(COOH) (blue) and UiO-66(Zr)-(COOH)₂ (red) ($\lambda_{\text{Cu}} \sim 1.54059 \text{ \AA}$) compared with the ones calculated from simulated structures (grey).

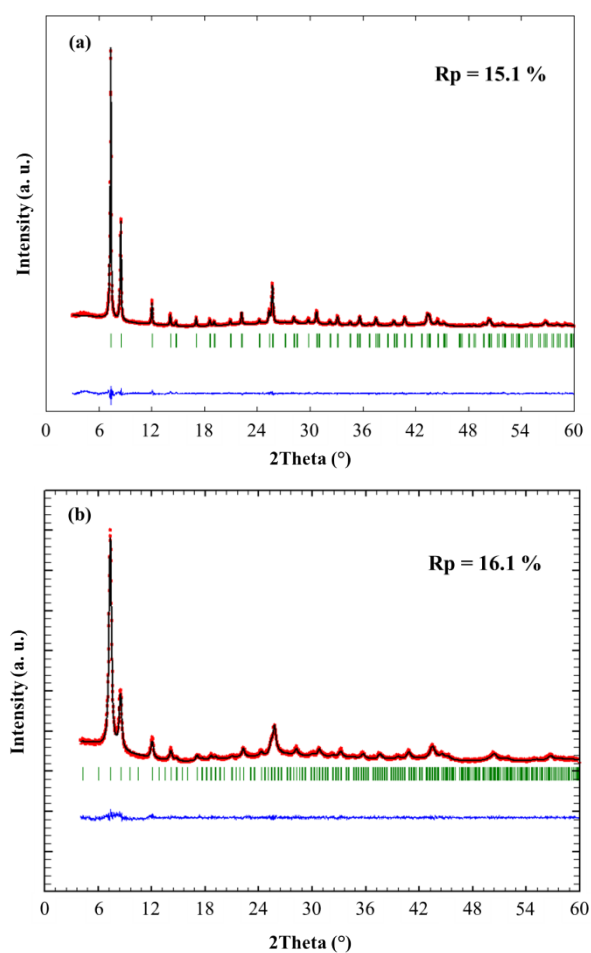


Figure S2. Structureless pattern profile refinement plot of (a) UiO-66(Zr)-(COOH) and (b) UiO-66(Zr)-(COOH)₂ ($\lambda_{\text{CuK}\alpha} = 1.54059$). Red: experimental points; black: calculated points;

green: Bragg peaks; blue: difference pattern (exp.-calc.). The profile factor Rp has been indicated on each figure.

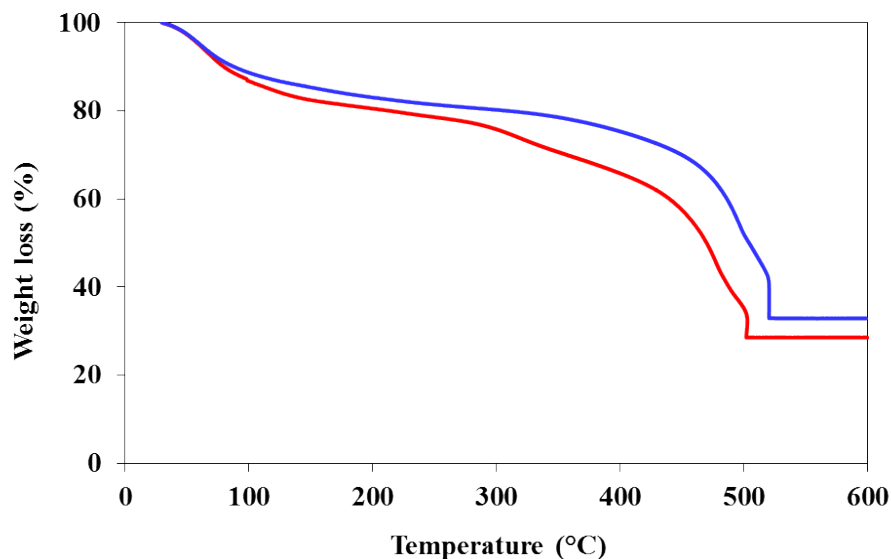


Figure S3. Thermo-Gravimetric analysis of UiO-66(Zr)-(COOH) (blue) and UiO-66(Zr)-(COOH)₂ (red) under O₂ (20 ml.min⁻¹; 2°C min⁻¹).

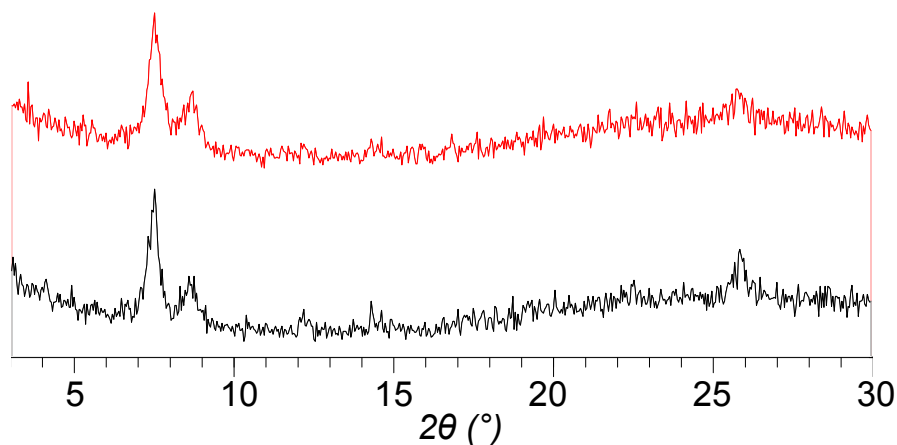


Figure S4. X-ray powder diffraction patterns of UiO-66(Zr)-(COOH)₂: as synthesized (black) and after activation at 180°C and re-dispersion in water (red) ($\lambda_{Cu} \sim 1.54059 \text{ \AA}$). (Acquisition time : 15 min).

Elemental analysis

Elemental analyses (C, H, Zr) were performed by the service central d'analyse, CNRS, Vernaison, France. C and H contents were determined by analysing the amount of CO₂ and H₂O released after the total combustion of the sample (under O₂ at 1050°C), while the Zr content was evaluated by ICP-AES analysis after the dissolution of the sample in acidic medium.

The amount of adsorbed H₂O in the title solids depends on the ambient conditions (temperature, humidity); this amount was thus adjusted to match the absolute % values. Nevertheless, only the experimental C/Zr ratio was used to determine the accurate formula (and assess the potential sub-stoichiometry of ligand). A slight substoichiometry may thus be possible for UiO-66-(COOH).

Table S4. Elemental analysis of the title compounds and calculated values for possible stoichiometric formulas.

Formula	C (wt %)		H (wt %)		Zr (wt %)		C/Zr (molar)	
	exp.	calc.	exp.	calc.	exp.	calc.	exp.	calc.
UiO-66-(COOH)	24.42		3.36		23.89		7.8	
Zr ₆ O ₄ (OH) ₄ (C ₉ H ₄ O ₆) ₆ (H ₂ O) ₄₀		24.49		4.11		20.67		9.0
Zr ₆ O ₄ (OH) ₄ (C ₉ H ₄ O ₆) _{5.2} (OH) _{1.6} (H ₂ O) ₃₀		24.51		3.62		23.87		7.8
UiO-66(Zr)-(COOH)₂	24.75		2.97		18.75		10.0	
Zr ₆ O ₄ (OH) ₄ (C ₁₀ H ₄ O ₈) ₆ (H ₂ O) ₄₀		24.74		3.74		18.79		10.0

3. Kinetic data

Normalized crystallization curves (α) were extracted from time dependent EDXRD patterns for both compounds by the integration of the (111) Bragg peaks at different temperatures. Induction time t_0 as well as the crystallization time t_f were extracted and are summarized in Table S4.

Crystallization curves were further analyzed using two models. The first one is the Avrami-Erofe'ev equation (AE) which relates the extent of crystallization α to the reaction time t and the induction time t_0 (equation 1).^{1,2} This equation was further linearized using Sharp and Hancock method (SH) (equation 2),³ allowing the extraction of the Avrami exponent n_{SH} and the rate constant k_{SH} (Table S4).

$$\alpha = 1 - \exp(-k_{SH}(t-t_0))^{n_{SH}} \quad (1)$$

$$n(-\ln(1-\alpha)) = n_{SH} \ln k_{SH} + n \ln(t-t_0) \quad (2)$$

The second one is the Gualtieri model⁴ which considers nucleation and growth as distinct processes as can be seen in equation 3 where a and b are constants related to the nucleation and k_g and n the rate constant of the crystal growth and the dimension of the growth. Here, we set $n=3$ as the UiO-66(Zr) solids crystallizes under a cubic symmetry. The rate constant of nucleation k_n is then calculated by equation 4.

$$\alpha = \frac{1}{1 + \exp^{-(t-a)/b}} [1 - \exp^{-(k_g * t)^n}] \quad (3)$$

$$k_n = 1/a \quad (4)$$

Crystallization curves

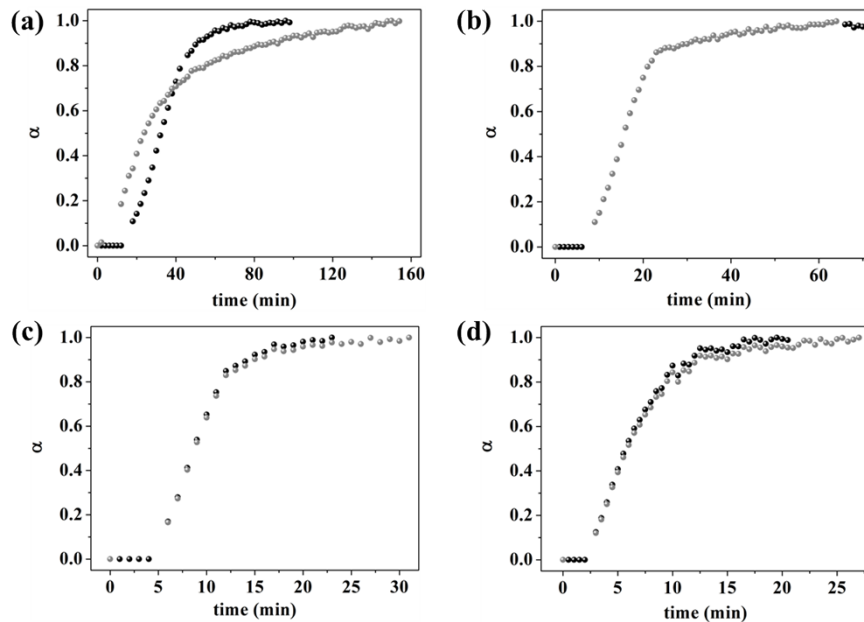


Figure S5. Comparison of crystallization curves of the phase UiO-66(Zr)-(COOH) (dark sphere) and UiO-66(Zr)-(COOH)₂ (grey sphere) synthesized at (a) 120 °C, (b) 130 °C, (c) 140 °C and (d) 150 °C.

Sharp-Hancock Analyses

Table S5. Crystallization time t_f , induction time t_0 and kinetics parameters (n_{SH} and k_{SH}) obtained by the Sharp-Hancock method with the Avrami-Erofe'ev equation of the UiO-66(Zr)-(COOH) and UiO-66(Zr)-(COOH)₂ synthesized at different temperatures. Values based on the integration of the (111) Bragg peak.

Temperatures	t_f (min)	t_0 (min)	Step 1	$n_{SH}(1)$	$k_{SH}(1)$ (min ⁻¹)	Step 2	$n_{SH}(2)$	$k_{SH}(2)$ (min ⁻¹)
UiO-66(Zr)-(COOH)								
110 °C	98	31	$0.1 < \alpha$	1.79	0.036	-	-	-
120 °C	78	15	< 0.95	1.58	0.046	-	-	-
130 °C	58	8	$0.1 < \alpha$ < 0.86	1.28	0.105	$0.86 < \alpha$ < 0.95	0.50	0.262
140 °C	21	5	$0.1 < \alpha$	1.20	0.217	-	-	-
150 °C	18	2	< 0.95	1.29	0.202	-	-	-
UiO-66(Zr)-(COOH)₂								
120 °C	142	6	$0.1 < \alpha$ < 0.95	0.85	0.036	-	-	-
130 °C	53	6	$0.1 < \alpha$ < 0.86	2.37	0.034	$0.86 < \alpha$ < 0.95	0.60	0.077
140 °C	25	4	$0.1 < \alpha$ < 0.83	1.90	0.037	$0.83 < \alpha$ < 0.95	1.02	0.087
150 °C	23	2	$0.1 < \alpha$ < 0.80	2.47	0.063	$0.80 < \alpha$ < 0.95	0.70	0.065

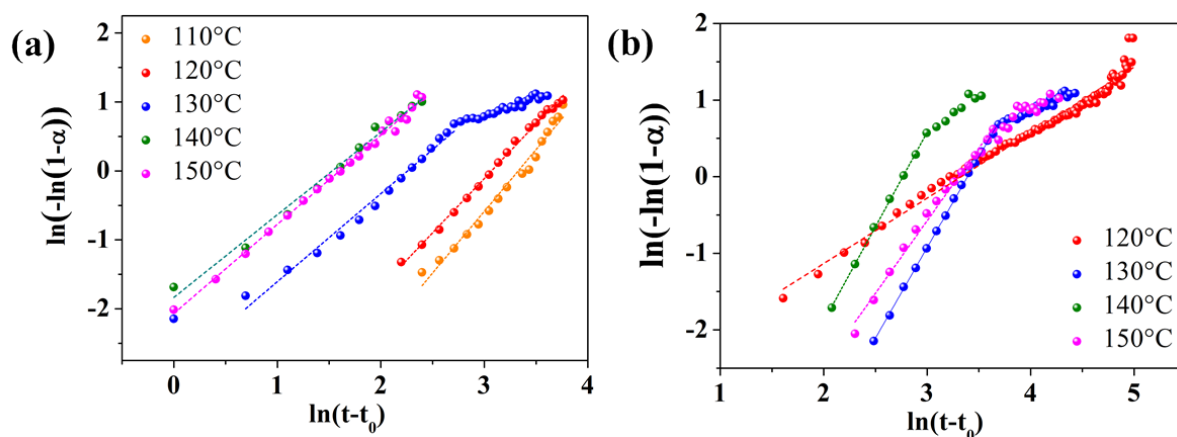


Figure S6. SH analyses using the AE nucleation-growth crystallization model of the phase (a) UiO-66(Zr)-(COOH) and (b) UiO-66(Zr)-(COOH)₂ synthesized at five different temperature.

Non-linear Gualtieri Analyses

Table S6. Kinetics parameters (a , b , k_g and k_n) obtained by the Gualtieri equation.

Temperatures	a (min)	b (min)	k_n (min ⁻¹)	k_g (min ⁻¹)
UiO-66(Zr)-CO₂H				
110 °C	54.1(9)	8.9(2)	0.02(0)	0.0185(3)
120 °C	29.4(2)	6.8(1)	0.0181(4)	0.0340(3)
130 °C	12.9(1)	2.6(1)	0.0262(5)	0.0775(6)
140 °C	7.85(9)	1.59(8)	0.061(2)	0.127(2)
150 °C	4.3(1)	1.5(1)	0.068(2)	0.233(6)
UiO-66(Zr)-(CO₂H)₂				
120 °C	10.6(8)	3.3(6)	0.0097(9)	0.09(8)
130 °C	12.9(1)	2.7(1)	0.0264(5)	0.0775(6)
140 °C	7.66(6)	1.60(6)	0.053(1)	0.131(1)
150 °C	4.00(8)	1.48(8)	0.0579(9)	0.250(5)

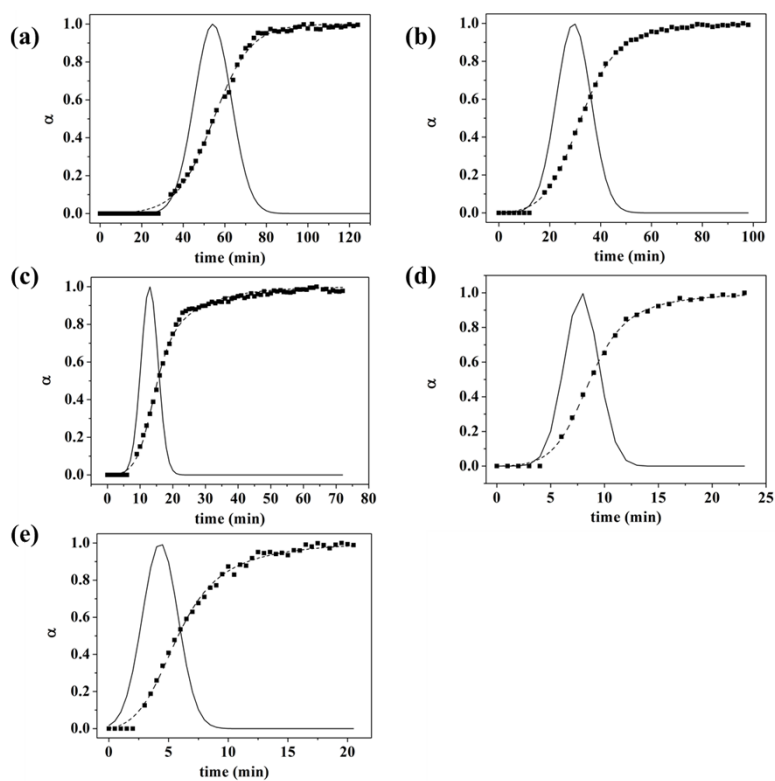


Figure S7. Extent of crystallization vs. time for the Bragg peak (111) of UiO-66(Zr)-(COOH) and corresponding non-linear least-squares fits with the Gualtieri equation as well as probability curves of nucleation PN.

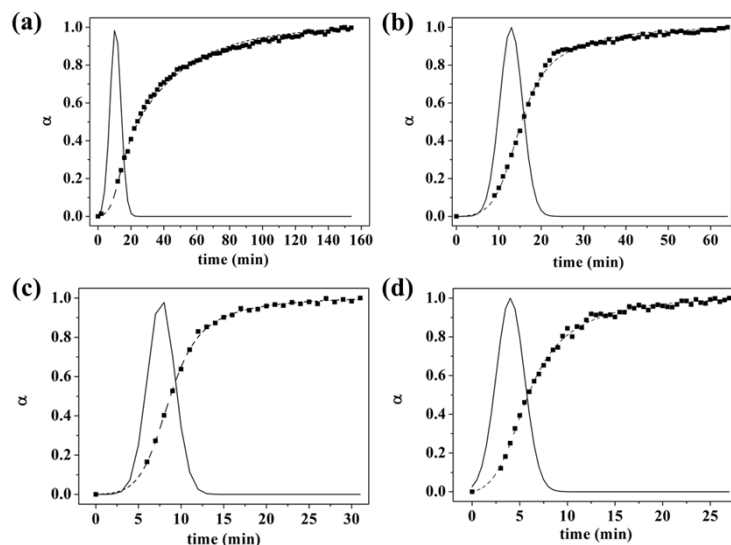


Figure S8. Extent of crystallization vs. time for the Bragg peak (111) of UiO-66(Zr)-(COOH)₂ and corresponding non-linear least-squares fits with the Gualtieri equation as well as probability curves of nucleation PN.

Arrhenius Plots

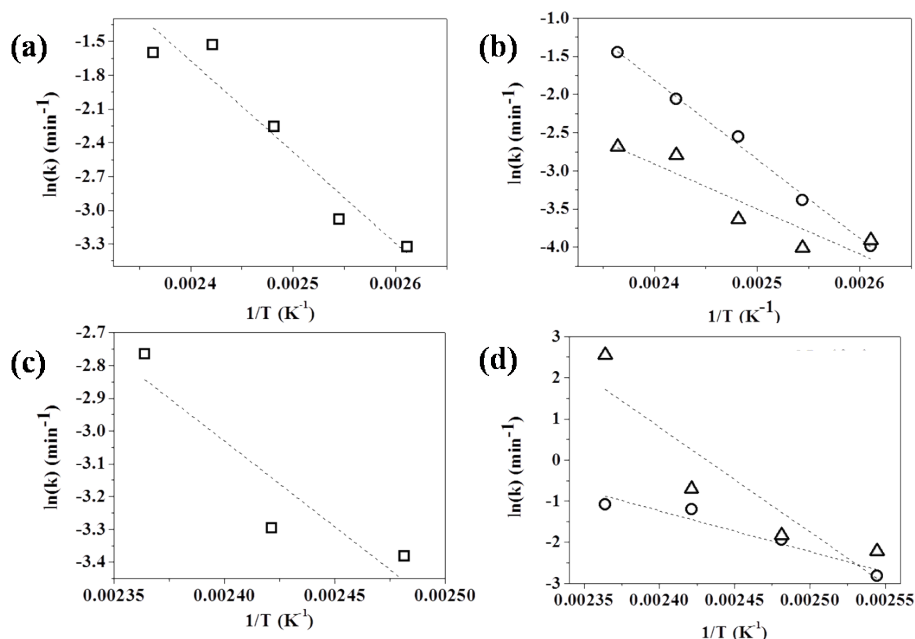


Figure S9. Arrhenius plots for the Bragg peak (111) for the temperature-dependant rate constants from the Avrami-Erofe'ev equation: (a) UiO-66(Zr)-(COOH) and (c) UiO-66(Zr)-(COOH)₂ and from the the Gualtieri model: (b) UiO-66(Zr)-(COOH) and (d) UiO-66(Zr)-(COOH)₂. (nucleation: round and growth: triangle)

4. Modelling

4.1 Methodology

4.1.1. DFT geometry optimization

The structural model of the anhydride form was geometry optimized as follows.

An energy minimization procedure was first employed to geometrically optimize this structure fixing the unit cell parameters to those of the UiO-66(Zr)-(COOH)₂. This was done using the Forcite module implemented in the Materials Studio software,⁵ based on the Universal force field (UFF)⁶ and the charges calculated via the Qeq charge equilibration method.⁷ Periodic density functional theory (DFT) geometry optimization procedure based on the hybrid B3LYP functional was further employed to refine the so-obtained structure using the CRYSTAL09 code,⁸ where both cell parameters and atomic positions were allowed to fully relax. In this calculation, all electron basis sets were used for each atom of the MOF framework. Basis sets for Zr and O were taken from Refs. ⁹ and ¹⁰ respectively, whereas for C and H atoms standard 6-31G(d, p) basis sets from Pople's family were adopted.¹¹ Polarization functions (one shell) were used on O, C and H atoms. For the numerical integration of the exchange–correlation term, extra large grid (XLGRID) in a Lebedev scheme was used, which corresponds to a pruned grid with 75 radial points and 974 angular points in the region of chemical interest. The condition for the SCF convergence was set to 10⁻¹⁰ Hartree during geometry optimization. The Pack–Monkhorst/Gilat shrinking factors for the reciprocal space were set to 2. The five truncation criteria (TOLINTEG) for the bielectronic integrals (Coulomb and HF exchange series) were set to 7 7 7 7 16. A modified Broyden scheme¹² following the method proposed by Johnson¹³ was utilized to accelerate the convergence in the self-consistent calculations after five SCF iterations, with 50% of Fock/KS matrices simple mixing and with the Johnson parameter set to 0.05. Such a DFT parameterization has been successfully employed to optimize the structures of UiO-66(Zr)¹⁴, its extended series¹⁵ as well as its functionalized forms.¹⁶

4.1.2. Theoretical Calculations of Pore volume and accessible Surface Area

For the optimized structures of the UiO-66(Zr)-(COOH)₂ and its anhydride form, the theoretical pore volumes (V_{pore}) were obtained according to the thermodynamic method proposed by Myers and Monson.¹⁷ In these calculations, UFF was used to describe the Lennard-Jones (LJ) interactions of the framework atoms while the LJ parameters for Helium

($\varepsilon/k_B = 10.9$ K, $\sigma = 2.64$ Å) were taken from the work of Talu and Myers.¹⁸ The accessible surface area (a_{acc}) is purely based on the geometric topology of the adsorbent and calculated from a simple Monte Carlo integration technique where the center of mass of the probe molecule with hard sphere is “rolled” over the framework surface.¹⁹ In this method, a nitrogen-sized (3.6 Å) probe molecule is randomly inserted around each framework atom of the adsorbent and the fraction of the probe molecules without overlapping with the other framework atoms is then used to calculate the accessible surface area. The LJ size parameters of the framework atoms were the same as those used for the calculations of the pore volume.

4.1.3. DFT calculations of the NMR isotropic chemical shifts

The calculations of the ^{13}C isotropic chemical shifts were performed with the CASTEP^{20,21} density-functional-theory (DFT)-based code available in the Materials Studio 5.0 package. The projector augmented waves (PAW)²² and gauge included projector augmented waves (GIPAW)²³ algorithms were used. The Perdew-Burke-Ernzerhof (PBE) functional²⁴ was used in the generalized gradient approximation (GGA) for the exchange correlation energy and the core-valence interactions were described by ultrasoft pseudopotentials.²⁵ The wave functions were expanded on a plane wave basis set with a kinetic energy cut-off of 600 eV. The Brillouin zone was sampled using a Monkhorst-Pack grid spacing of 0.04 \AA^{-1} (6 calculated k-points).

4.2 Correlation between NMR and modelling results

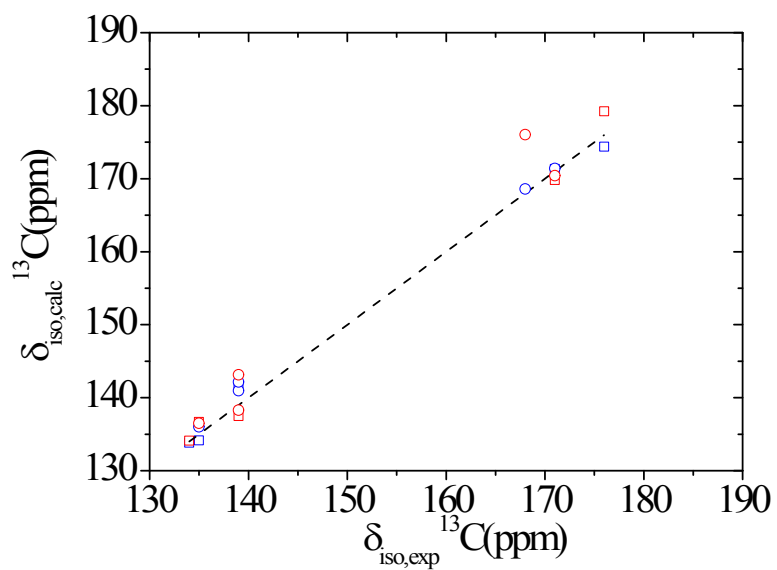


Figure S10. Correlation between NMR-measured and DFT-calculated ^{13}C isotropic chemical shifts. The blue and red symbols correspond to the calculations realized on the optimized and non-optimized structures respectively while the square and circle symbols are attributed to the data for UiO-66(Zr)-(COOH)₂ and to the anhydride form respectively.

5. Gas adsorption

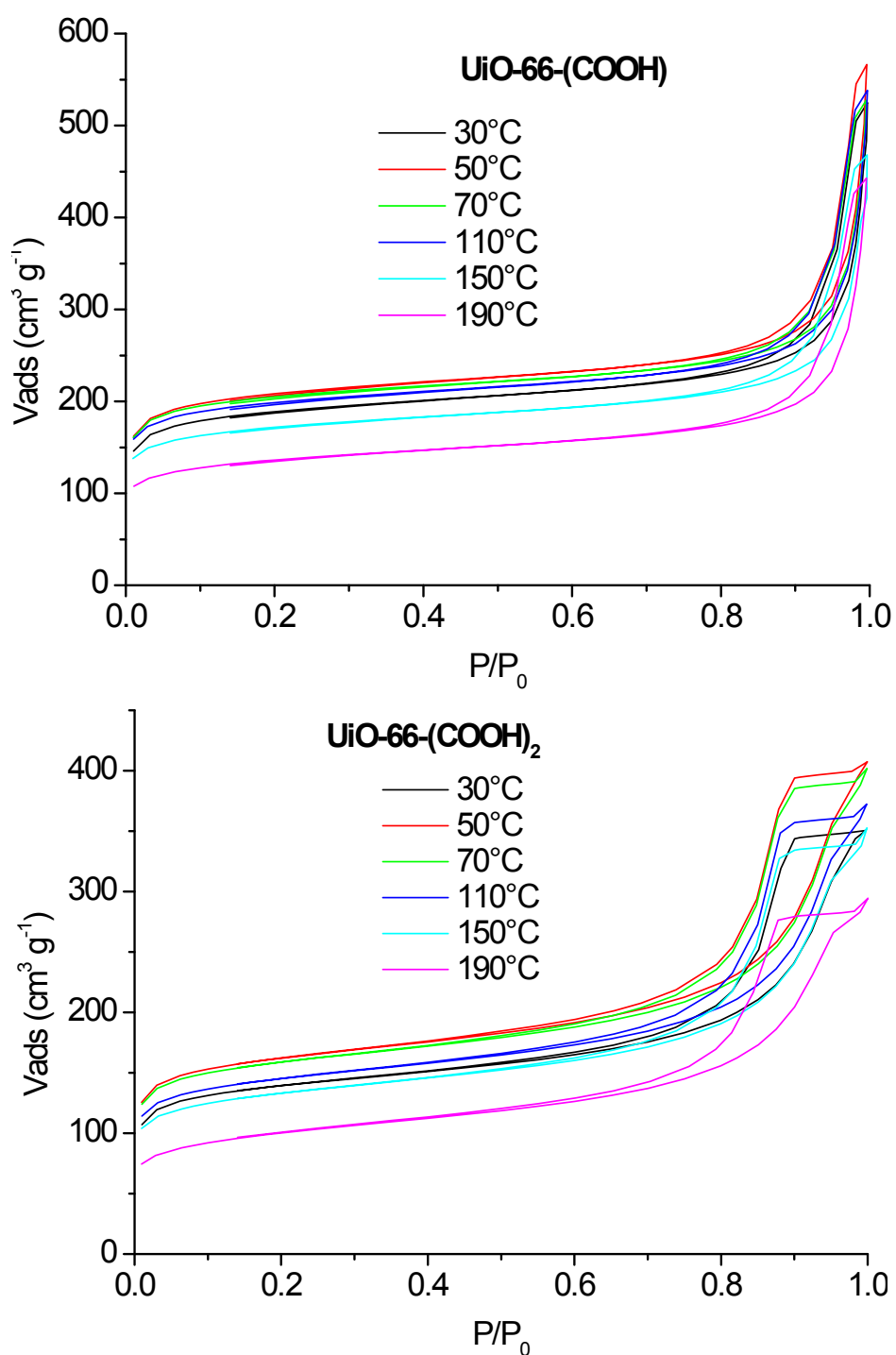


Figure S11. Nitrogen sorption isotherms (77 K) after activation at various temperatures. Top: UiO-66(Zr)-(COOH); bottom: UiO-66(Zr)-(COOH)₂.

Table S7. BET area and pore volume of UiO-66(Zr)-(COOH) and UiO-66(Zr)-(COOH)₂: dependence on the temperature of activation

Activation temperature (°C)	UiO-66(Zr)-(COOH)		UiO-66(Zr)-(COOH) ₂	
	a _{BET} (m ² g ⁻¹)	Micropore volume (cm ³ g ⁻¹)	a _{BET} (m ² g ⁻¹)	Micropore volume (cm ³ g ⁻¹)
30	661(17)	0.23(1)	453(11)	0.15(1)
50	673(18)	0.26(1)	527(13)	0.18(1)
70	661(18)	0.26(1)	516(13)	0.18(1)
110	642(18)	0.25(1)	473(12)	0.16(1)
150	556(15)	0.21(1)	435(13)	0.14(1)
190	443(11)	0.16(1)	332(7)	0.09(1)

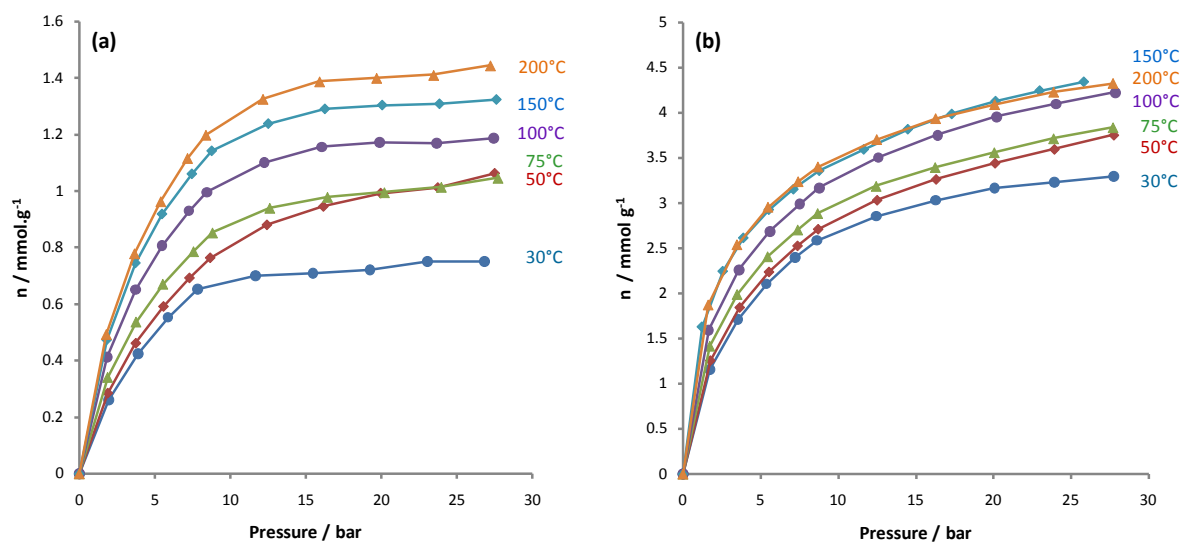


Figure S12. Isotherms obtained at 30°C with CH₄ (a) and CO₂ (b) for UiO-66(Zr)-(COOH)₂ outgassed at increasing temperatures.

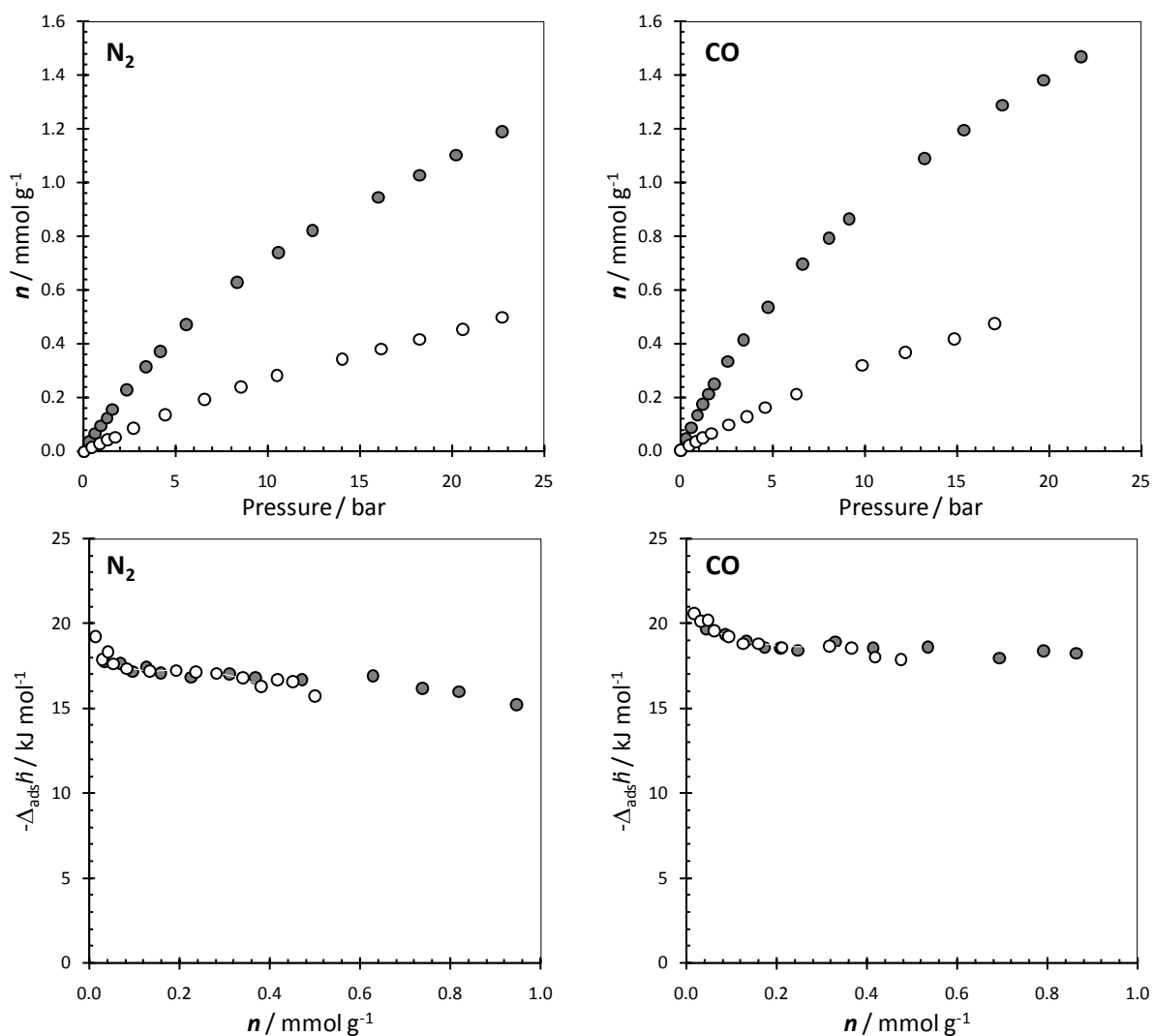


Figure S13. Isotherms (upper curves) and adsorption enthalpies (lower curves) obtained at 30°C with N₂ (left) and CO (right) for UiO-66(Zr)-(COOH)₂ outgassed to 30°C (○) and 150°C (●).

References

1. M. Avrami, *J. Chem. Phys.*, 1941, **9**, 177.
2. B. V. Erofe'ev, *Compt. Rend. Acad. Sci. URSS* 1946, **52**, 511.
3. J. D. Hancock and J. H. Sharp, *J. Am. Ceram. Soc.*, 1972, **55**, 74.
4. A. F. Gualtieri, *Phys. Chem. Min.*, 2001, **28**, 719.
5. Accelrys, Inc., Materials Studio, 3.0 V; Accelrys Inc: San Diego, CA, 2003.
6. A.K. Rappé, C.J. Casewit, K.S. Colwell, W.A. Goddard III and W.M. Skiff, *J. Am. Chem.*

- Soc.* 1992, **114**, 10024.
7. A. K. Rappé and W. A. Goddard III, *J. Phys. Chem.* 1991, **95**, 3358.
 8. R. Dovesi, V.R. Saunders, R. Roetti, R. Orlando, C.M. Zicovich-Wilson, F. Pascale, B. Civalleri, K. Doll, N.M. Harrison, I.J. Bush, P. D'Arco and M. Llunell, *CRYSTAL09*, University of Torino, Torino, 2009.
 9. http://www.crystal.unito.it/Basis_Sets/zirconium.html. (Zr_all_electron_dovesi_unpub).
 10. Y. Noel, C.M. Zicovich-Wilson, B. Civalleri, P. D'Arco and R. Dovesi, *Phys. Rev. B: Condens. Matter* 2002, **65**, 014111.
 11. <https://bse.pnl.gov/bse/portal>.
 12. C.G. Broyden, *Math. Comput.* 1965, **19**, 577.
 13. D. D. Johnson, *Phys. Rev. B* 1988, **38**, 12807.
 14. L. Valenzano, B. Civalleri, S. Chavan, S. Bordiga, M. H. Nilsen, S. Jakobsen, K. P. Lillerud and C. Lamberti, *Chem. Mater.*, 2011, **23**, 1700.
 15. Q. Yang, V. Guillerm, F. Ragon, A. D. Wiersum, P. L. Llewellyn, C. Zhong, T. Devic, C. Serre and G. Maurin, *Chem. Commun.*, 2012, **48**, 9831.
 16. D. Wu, Q. Yang, C. Zhong, D. Liu, H. Huang, W. Zhang and G. Maurin, *Langmuir* 2012, **28**, 12094.
 17. A.L. Myers and P.A. Monson, *Langmuir* 2002, **18**, 10261.
 18. O. Talu and A.L. Myers, *AIChE J.* 2001, **47**, 1160.
 19. T. Düren, F. Millange, G. Férey, K. S. Walton and R. Q. Snurr, *J. Phys. Chem. C*, 2007, **111**, 15350-15356.
 20. M. D. Segall, P.L.D. Lindan, M.J. Probert, C.J. Pickard, P.J. Hasnip, S.J. Clark and M.C. Payne, *J. Phys.: Condens. Matter* 2002, **14**, 2717.
 21. S.J. Clark, M.D. Segall, C.J. Pickard, P.J. Hasnip, M.J. Probert, K. Refson, and M.C. Payne, *Z. Kristallogr.* 2005, **220**, 567.
 22. M. Profeta, F. Mauri, and C.J. Pickard *J. Am. Chem. Soc.* 2003, **125**, 541.
 23. C.J. Pickard and F. Mauri, *Phys. Rev. B* 2001, **63**, 245101.
 24. J.P. Perdew, K. Burke and M. Ernzerhof, *Phys. Rev. Lett.* 1996, **77**, 3865.
 25. J.R. Yates, C.J. Pickard and F. Mauri, *Phys. Rev. B* 2007, **76**, 024401.